

X-ray analysis of wurtzite-type CoO(111) films on Ir(001): Correlation of structure, stress, electronic, and magnetic properties

Sumalay Roy,¹ H. L. Meyerheim,^{1,*} K. Mohseni,¹ Z. Tian,¹ D. Sander,¹ M. Hoffmann,^{2,1} W. Adeagbo,² A. Ernst,^{1,3} W. Hergert,² R. Felici,⁴ and J. Kirschner^{1,2}

¹Max-Planck-Institut für Mikrostrukturphysik, Weinberg 2, D-06120 Halle, Germany

²Institut für Physik, Martin-Luther-Universität Halle-Wittenberg, D-06099 Halle, Germany

³Wilhelm Ostwald Institut für Physikalische und Theoretische Chemie, Universität Leipzig, Linnéstrasse 2, D-04103 Leipzig, Germany

⁴ESRF, B.P. 220, F-38043 Grenoble Cedex, France

(Received 17 February 2014; revised manuscript received 8 April 2014; published 29 April 2014)

We present a surface x-ray diffraction study in combination with stress experiments and *ab initio* calculations to investigate the structure and magnetic properties of 1.6 and 2.0 bilayer thick CoO(111) films grown on Ir(001). The CoO films grow in a wurtzite-like structure characterized by reduced distances between cobalt and oxygen atoms within one bilayer. The double-bilayer film is under tensile stress of +2.1 N/m which can be quantitatively attributed to epitaxial misfit and excludes the presence of significant Coulomb interactions. First-principles calculations reveal that the CoO films are metallic and that the magnetic order is noncollinear.

DOI: [10.1103/PhysRevB.89.165428](https://doi.org/10.1103/PhysRevB.89.165428)

PACS number(s): 68.35.Ct, 68.35.Gy, 71.15.Mb, 79.60.Dp

I. INTRODUCTION

Ultrathin films of CoO have been intensely studied in recent years because of their intriguing structural and magnetic properties [1–6]. This is also due to the intimate relation between structure and magnetic properties and the large variety of structures observed for ultrathin CoO films depending on stoichiometry and film thickness. Also, epitaxial CoO films have shown a remarkable dependence of their magnetic properties on the strain imposed by the supporting substrates [7].

The rocksalt (RS) structure has been proposed as the structure model for bulk CoO [8]. In this model, the structure along the [111] direction is composed of alternating layers of Co and oxygen atoms, where one Co-O sequence is called a *bilayer*. Co and O atoms are stacked in an fcc-like ABCAB... fashion. In view of the ionic nature of Co and O, a permanent dipole moment arises at the (111) face, leading to the divergence of the electrostatic potential. According to the classification by Tasker [9], CoO(111) is a so-called type III structure, which is inherently unstable. In contrast to the expectation, CoO(111) samples exist and are stable.

Several charge compensation mechanisms have been discussed in the past to provide insight into the stability of this structure. Surface reconstructions, charge transfer, and the adsorption of foreign species [10,11] have been proposed as factors contributing to the stability. Although originally developed for bulk crystals, it has been shown recently that also for ultrathin films, for which no actual divergence of the electrostatic potential exists, bulklike charge compensation mechanisms can exist [12–14].

On the other hand, in ultrathin films different compensation mechanisms have been proposed, where a change of the atomic structure is considered. One example is the transition from the wurtzite (WZ) structure to the hexagonal boron nitride (h-BN) structure of ZnO grown on Ag(111) [15,16] and the

presence of the WZ stacking near the surface of a several bilayer thick CoO film on Ir(001) [4] and on Pt(111) [17]. This change of structure is related to the metallization of the surface. On the other extreme, for a single CoO(111) bilayer, ordered patches of a h-BN type and a RS type CoO phase were proposed [1]. This model was later corroborated by scanning tunneling microscopy and density functional theory (DFT) calculations [5,6].

While the previous studies have clearly revealed the complex nature of the structure of CoO films of one bi-layer and in the “thick” film limit, no study for an intermediate film thickness such as a double bilayer thick film has been carried out. In this paper we present a surface x-ray diffraction (SXRD) analysis of a 1.6 and 2.0 bilayer thick CoO film grown on Ir(001). The structural characterization is supplemented by stress measurements and *ab initio* theory to address forces acting in the CoO films and to provide an electronic picture of the underlying phenomena, respectively.

We find that both films form a c -(10 \times 2) superstructure within an accuracy of the spot position in the range of 10⁻³ reciprocal lattice units, using a substrate rod as reference. The CoO films are characterized by a WZ-like structure. Co atoms, which are next to the Ir(001) surface at an interatomic distance in the range between 2.4 Å and 2.5 Å, are located in asymmetric positions away from hollow sites. Vertical intralayer distances within a bilayer are equal to $u_i = 0.99$ Å and $u_s = 0.49$ Å for the 1.6 and to $u_i = 0.86$ Å and $u_s = 0.20$ Å for the 2.0 bilayer film, respectively. Subscripts (i) for interface and (s) for surface refer to the bilayer next to the Ir(001) substrate and the top layer, respectively. Comparison with the bulk value in the RS structure ($u = 1.23$ Å) indicates significant reduction which might be related to the depolarization of the structure. The structure model is supported by the quantitative analysis of our stress measurements, which indicate that the measured stress is induced by lattice misfit, and there is no indication of significant repulsive Coulomb interactions. *Ab initio* calculations reveal a metallic character of the whole film and a noncollinear magnetic structure.

*hmeyerhm@mpi-halle.mpg.de

II. EXPERIMENT

A. Surface x-ray diffraction

In situ growth of CoO on Ir(001) followed by SXR characterization were carried out at the ID03 beamline of the European Synchrotron Radiation Facility (ESRF) in Grenoble, France [18]. We used a six-circle ultrahigh vacuum diffractometer operated in the z -axis mode. The intensity distribution along the superlattice rods was measured under grazing incidence ($\alpha_i = 3^\circ$) of the incoming x-ray beam ($\lambda = 0.69 \text{ \AA}$) by rotating the sample about the surface normal. The angle of incidence of the incoming x-ray beam was deliberately chosen to be much larger than the critical angle of the total external reflection in order to avoid systematic errors due to possible misalignment of the small samples.

The superlattice rods arise due to the two-dimensional nature of thin films, which makes the third reflection index, $l = q_z/c^*$, a continuous parameter. Here, q_z and c^* represent the momentum transfer normal to the surface and reciprocal lattice unit, respectively [19–21].

The CoO(111) films were prepared by deposition of Co followed by annealing in an oxygen atmosphere. The Co source was calibrated by SXR as shown in Fig. 1. The reflection intensity at the position (0 1 0.2), i.e., close to the antiphase scattering position (0 1 0), is monitored. The first and second Co layer is completed after $\Delta t \approx 400 \text{ s}$ and another $\Delta t \approx 300 \text{ s}$ after starting the deposition at $t \approx 200 \text{ s}$, respectively. In the following, the Co film was oxidized by annealing the sample to 600 K in an oxygen atmosphere at a partial pressure of $2 \times 10^{-6} \text{ mbar}$ by simultaneously monitoring one superlattice characteristic for the c -(10 \times 2) superstructure [(9 1); see below]. For the SXR experiments two samples were prepared with thicknesses, as derived *ex posteriori* by SXR analysis, of 1.6 and 2.0 bilayers of CoO.

B. Stress measurement

We measure the stress-induced change of curvature of a thin Ir(001) single crystal by an optical two-beam deflection technique under UHV conditions, which has been described before [22,23]. In short, the deposition of Co on Ir(001) leads to an epitaxial misfit induced film stress on the order of several

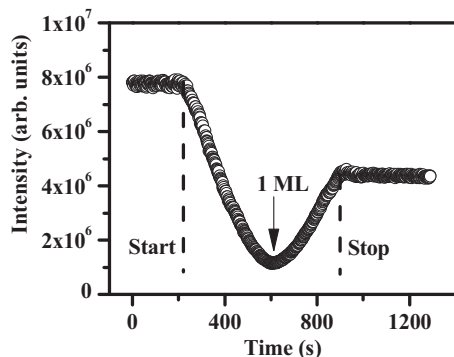


FIG. 1. Intensity of the antiphase (010) diffraction peak versus time during deposition of 2 ML Co at 300 K. Vertical lines marked “start” and “stop” indicate when the shutter of the Co evaporator was opened and closed, respectively.

GPa, and this induces a change of curvature of the 0.1 mm thin substrate crystal with a radius of the curvature on the order of 400 m. The stress, which induces the curvature change, is quantitatively extracted from monitoring the deflection of two laser beams on position-sensitive detectors upon reflection at the curved substrate surface [23]. The overall error bar for the derived film stress is $\pm 5\%$.

As outlined in the results section, the stress measurement of the CoO film is carried out using a two-step process, where we measure first the film stress upon Co deposition at 300 K. Then, the stress change of the 2 ML Co/Ir(001) system upon subsequent oxidation by exposure to an O_2 partial pressure of $2 \times 10^{-6} \text{ mbar}$ for an equivalent of 400 L [1 L = 1 Langmuir ($1.33 \times 10^{-6} \text{ mbar s}$)] at 600 K is detected. Comparable results are also obtained by stress measurements during Co deposition in an O_2 partial pressure at 600 K. Stress measurements at elevated temperature in an oxygen atmosphere have been performed successfully recently for NiO/Ag(001) [24], but here we focus on the two-step process since this is the preparation procedure employed in the SXR experiments. It also allows us to interrupt the oxygen exposure at any point to monitor the progress of the Co oxidation by *in situ* LEED [25]. The investigation of the LEED pattern confirms that the c -(10 \times 2) CoO(111) structure has formed after an exposure to 400 L O_2 at the given experimental conditions.

III. RESULT AND DISCUSSION

A. SXR analysis

Figure 2 shows a schematic of the reciprocal space in the a^* - b^* plane of the Ir(001) surface. Large circles represent the Ir substrate crystal truncation rods, while large pentagons and small circles are related to superlattice (SL) rods of the CoO film forming a c -(10 \times 2) superstructure. We emphasize that

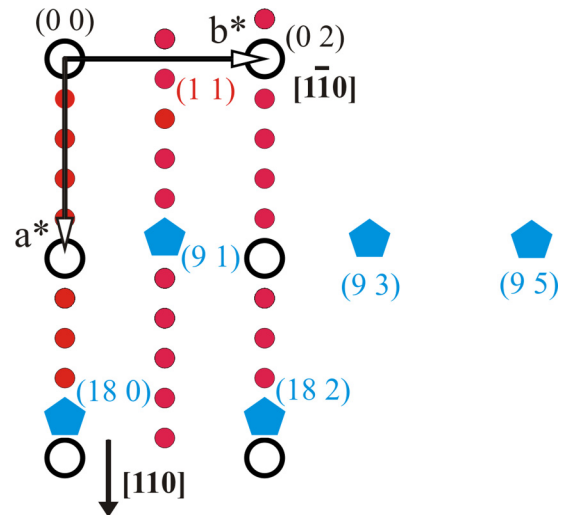


FIG. 2. (Color online) Schematic of the reciprocal space lattice in a projection along the bulk [001] direction. Large circles represent (1 \times 1) Ir crystal truncation rods. Filled small circles and pentagons represent CoO superlattice rods indexed according to the c -(10 \times 2) superstructure. Only the rods labeled by pentagons were used for the analysis; see text.

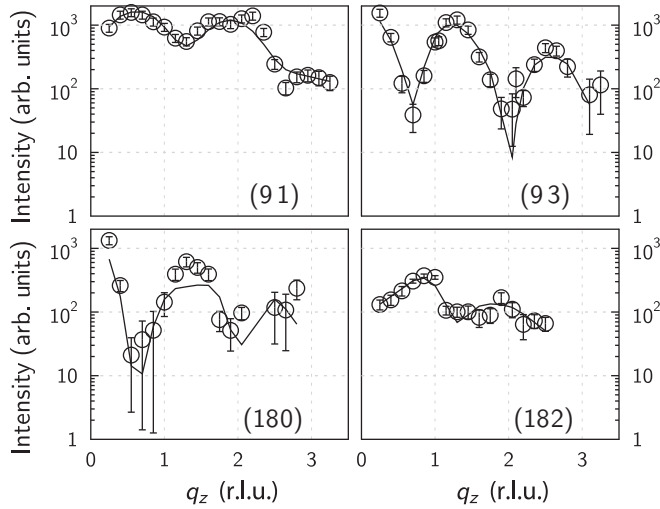


FIG. 3. Measured (symbols) and calculated (lines) intensities along different superlattice rods for the 1.6 bilayer sample. Indexing of the rods refers to the c -(10×2) unit cell (see Fig. 2).

for clarity only one of two rotational domains is shown. Rods are indexed according to the c -(10×2) superstructure. With the exception of the (1 1) rod, we found that only those rods which are labeled by pentagons had enough intensity to be detected by SXRD. The consideration of these rods only is equivalent to projecting the structure related to the c -(10×2) into a small c -(1×2) unit cell.

This simplification neglects the modulation of the atomic positions along the different crystallographic directions, i.e., along the [110] (a axis), $[1\bar{1}0]$ (b axis), and the [001] (c axis), which in the case of the single-bilayer film has been found to be substantial being on the order of several tenths of an Å [1]. Since a similar modulation can be expected in our film also, the “projection” of the c -(10×2) onto the c -(1×2) unit cell requires the proper description of the resulting static disorder. We considered this by applying anisotropic atomic displacement factors $T(hkl)$ for the individual atoms [26]. The importance of $T(hkl)$ for the SXRD analysis is most evident by considering the modulation along [110] as shortly explained in the following.

The deviation from the average structure is the reason for the appearance of SL reflections indicated by red dots in Fig. 2. Their finite intensity is missing in the “main” reflections labeled by pentagons which correspond to the average structure related to the c -(1×2) unit cell. In the analysis of modulated structures, models have been developed using simple sinusoidal modulations of the atomic positions. Here, the intensities of the main ($n = 0$) and satellite reflections of n th order are proportional to the square of the Bessel functions of order n : $I_n(\mathbf{q}) \propto |J_n(\mathbf{q} \cdot \mathbf{u})|^2$, where \mathbf{u} represents the modulation vector and the scattering vector \mathbf{q} is given by $\mathbf{q} = h\mathbf{a}^* + k\mathbf{b}^* + l\mathbf{c}^*$ assuming a Cartesian coordinate system and reciprocal axes $\mathbf{a}^*, \mathbf{b}^*, \mathbf{c}^*$ [27]. In the context of the analysis of the film structures, to first order the intensity reduction in the main reflections represented by $|J_0(\mathbf{q} \cdot \mathbf{u})|^2$ is approximated by the damping factor $T(hkl)$ (see in detail below).

Solid symbols in Figs. 3 and 4 represent the experimentally derived intensity distribution [$I_{\text{obs}}(hkl)$] along the different

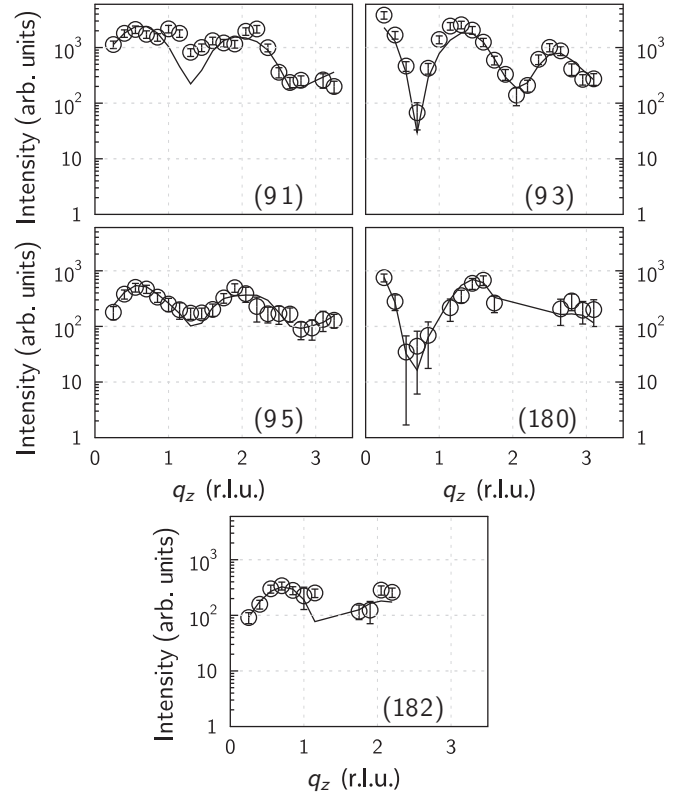


FIG. 4. Measured (symbols) and calculated (lines) intensities along different superlattice rods for the 2.0 bilayer sample. Indexing of the rods refers to the c -(10×2) unit cell (see Fig. 2).

SL rods for the 1.6 and 2.0 bilayer sample, respectively. Data sets consist of 75 and 86 reflections along four and five SL rods after averaging symmetry equivalent reflections (two per reflection). Solid lines represent the calculated reflection intensities [$I_{\text{calc}}(hkl)$], derived from the models outlined below. Uncertainties (1σ) shown as error bars were derived from the sum of the statistical uncertainties and the reproducibility of symmetry equivalent reflections as described by Robinson [28]. On the average, uncertainties lie in the 10% to 15% range (based on intensities, not structure factors), which is reasonably good especially in view of the low intensities involved.

The structure refinement was carried out using the program PROMETHEUS [29], allowing refinement of anisotropic displacement factors [26]. We started by considering the c -(1×2) unit cell using the structure model proposed by Mittendorfer *et al.* [5] for a single-bilayer film. Here, the registry of the oxygen and Co atoms of the first bilayer is defined by top sites (oxygen) and hollow/bridge sites (Co), respectively. This is shown in Fig. 5 which outlines the structure models for the 1.6 (a) and the 2.0 (b) bilayer film in top view. Large (red) and small (blue) balls represent oxygen and Co atoms, respectively. Atoms in light contrast are beneath those which are represented by stronger contrast. Also, the first two Ir layers (large, yellowish balls) are included. In order to clarify the atomic structure, several unit cells along the [110] direction are shown.

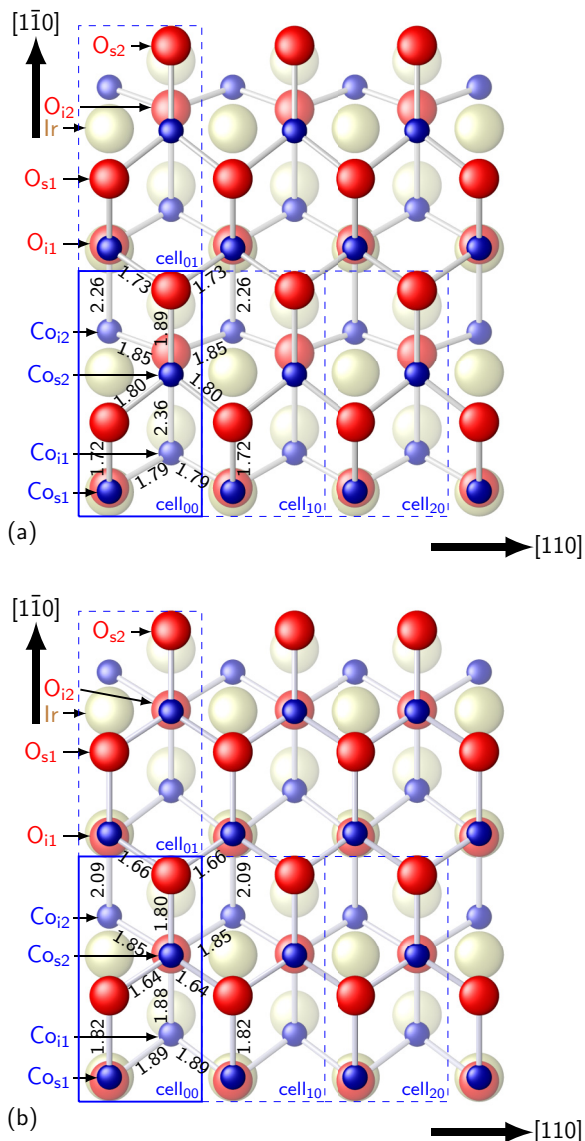


FIG. 5. (Color online) Top view of the structure model of the 1.6 (a) and 2.0 (b) bilayer CoO film on Ir(001). Red, blue, and yellowish balls represent the O, Co, and Ir atoms, respectively. Atoms in lighter color are below those represented in darker color. The rectangle (solid blue) represents the size of the $p-(1 \times 2)$ unit cell. Distances are given in Å units. Atoms in the bilayer next to the Ir(001) substrate are labeled by (i) while atoms in the top bilayer are labeled with (s).

In the context of the SXRD analysis two issues are important to note: (i) The CoO film also forms in a geometry related to the mirror image of the structure shown, where the mirror is parallel to the $[110]$ direction. Thus, in the analysis an incoherent average over two twin domain structures has to be carried out. Both domains are present in an equal fraction. (ii) The plane group symmetry changes from $c-(1 \times 2)$ to $p-(1 \times 2)$ if the Ir(001) substrate crystal is taken into account. As long as the Ir atoms remain on bulk (1×1) positions, they do not contribute to the SL rods and the unit cell can be considered as a centered one. In this case SXRD reflections fulfill the condition $(h + k = 2n, n \text{ integer})$ for their appearance.

The consideration of a single bilayer was not sufficient to fit the measured data. As can be seen in Figs. 3 and 4 the sinusoidal modulation of the intensity along q_z suggests a two-layer structure. Consequently, a second CoO bilayer was added. The atomic positions of all atoms along the $[1\bar{1}0]$ direction and along the surface normal $[001]$ were allowed to vary in addition to the fractional occupancy of the top layer atoms (θ_{Co} , θ_{O}) thereby preserving the Co : O = 1 : 1 stoichiometry. By contrast, the positions of the atoms along the $[110]$ direction were kept fixed due to their location on a mirror line.

Good fits were obtained on the basis of these structure models. As can be seen in Figs. 3 and 4, $I_{\text{calc}}(hkl)$ follows $I_{\text{obs}}(hkl)$ very well throughout the whole range of q_z , where the intensity varies over almost four orders of magnitude. The quality of fit is quantified by two parameters, the unweighted residual (R_u) and the goodness of fit (GOF) [30]. We find GOF values of 1.61 and 1.60 for the 1.6 and the 2.0 bilayer film, respectively, corresponding to R_u in the 20% to 25% range (note that R_u is based on intensities rather than on structure factors).

The structure models derived from the SXRD analysis are shown in Figs. 5–7 in top view and in side view along two different azimuths. In general we find that both CoO films are characterized by a WZ-like structure, where the Co atoms are located at the interface to the Ir(001) surface. The film structure resembles to that in the upper two bilayers of the CoO(111) film studied by Meyer *et al.* [4]. In this work the quantitative LEED analysis of a film which was prepared by oxidizing a five monolayer equivalent thick Co film indicated a RS structure followed by a stacking fault involving the switch to the WZ structure. It was argued that the switch to the WZ structure is related to the polarity compensation by creating a metallic surface [31]. As will be discussed later in the theory section, we expect a metallic behavior for our CoO films.

With regard to the polarity compensation mechanism in ultrathin films, also the efficient displacive WZ to h-BN transition has been observed for ZnO films on Ag(111) [16], albeit not a complete one. By contrast, it was shown that CoO nanocrystals embedded in the ZnO matrix do not transform to the h-BN structure but rather keep their WZ structure [15]. Our analysis shows that the CoO films show some tendency to convert from the WZ to the h-BN structure. This is most pronounced at the top bilayer and in the case of the 2.0 bilayer sample (see Fig. 6). The vertical spacings between the oxygen and the Co atoms are indicated in Å units. They amount to $u_i = 0.99$ Å and $u_s = 0.49$ Å for the 1.6 and $u_i = 0.86$ Å and $u_s = 0.20$ Å for the 2.0 bilayer sample, respectively. Uncertainties for distance determinations generally lie in the 0.05 Å to 0.10 Å range. In this respect our double-bilayer films are distinctly different from the single-bilayer film studied by Ebensperger [1] and Mittendorfer [5], where both patches of h-BN and a RS structure were found. Consequently we can conclude that with the growth of a second bilayer a structural reorganization sets in, which lifts the h-BN type geometry within the first bilayer.

In agreement with Mittendorfer *et al.* [5] we find that the registry between film and substrate shown in Fig. 5 has a small preference as compared to that where the CoO registry is shifted by half a unit cell along $[110]$. However, the difference

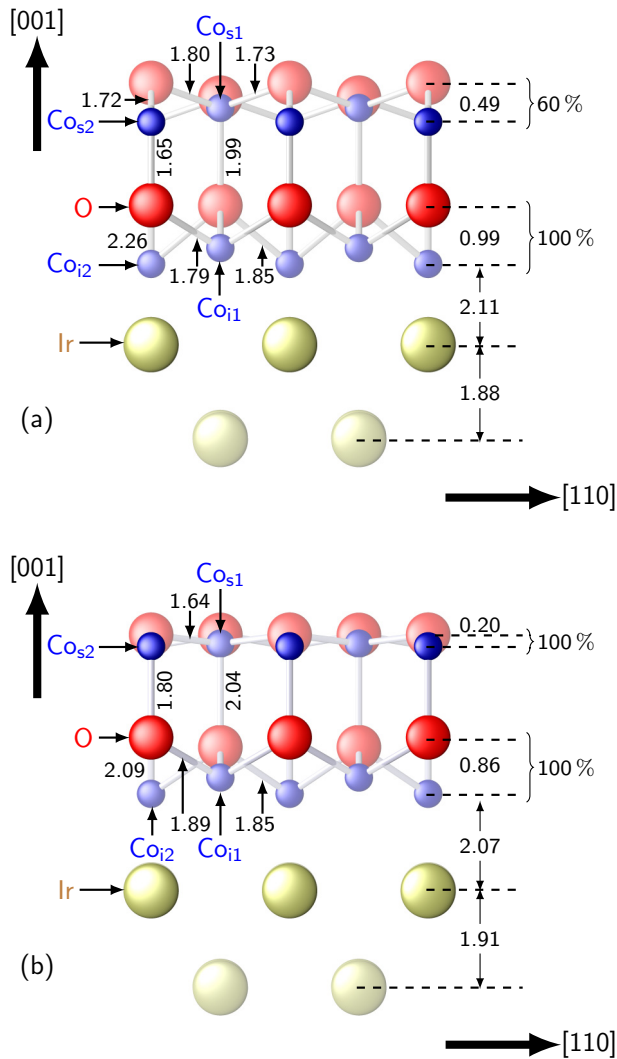


FIG. 6. (Color online) Side view of the 1.6 (a) and 2.0 (b) bilayer CoO film on Ir(001). Labels are identical to those in Fig. 5. Fractional occupancy factors are indicated on the right.

in the fit quality is small: GOF = 1.69 for the shifted registry versus 1.60 for the best fit. Given the approximations in our analysis we do not claim this difference in the GOF to be significant enough to allow clear-cut conclusions.

An overall common property of ultrathin CoO films is that the Co-O interatomic distances are short. As can be seen in Figs. 5–7, we derive values between 1.64 Å (minimum) and 2.36 Å (maximum), but a closer look shows that the majority of the distances lies in the 1.70 Å to 1.90 Å range. One can compare these values with those of the respective bulk structures, which are equal to 2.135 Å in the RS structure and 1.93 Å and 2.16 Å in the WZ structure for the in-plane and out-of plane bonds, respectively [31]. Short Co-O distances is a general observation in ultrathin CoO films. Ebensperger *et al.* [1] found values in the 1.81 Å to 2.01 Å range, while Meyer *et al.* [4] published 1.89 Å and 1.91 Å for the vertical Co-O distance within the WZ-type structure of their “thin” and “thick” film, respectively. Bond contractions by 5% to 10% do not come as a surprise, given the reduced coordination of surface and interface atoms.

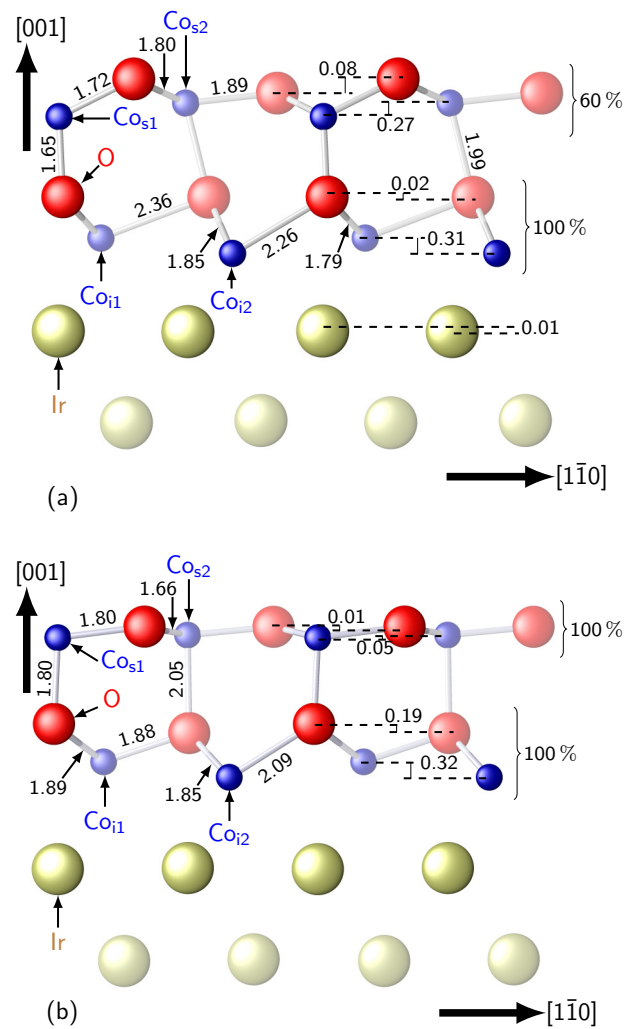


FIG. 7. (Color online) Side view of the 1.6 (a) and 2.0 (b) bilayer CoO film on Ir(001). Labels are identical to those in Fig. 5.

The Co-Ir bonds are not shown for clarity. We find values in the range between 2.4 Å to 2.5 Å, rather close to those derived for Co films grown on Ir(100)-(1×1) [32]. The Ir-Ir distances are 2.75 Å, and this corresponds to the equilibrium bond length in bulk Ir. Along the [110] direction surface Ir atoms are only very slightly (≈ 0.05 Å) displaced out of their bulk positions. However, this is significant enough to contribute to the SL rods. We emphasize that this converts the centered unit cell to a primitive one even in the case of a centered CoO film structure, and that only this allows the analysis of the registry between CoO film and substrate. Top-layer spacings within the Ir substrate ($d = 1.88$ Å and 1.91 Å) are not relaxed within the accuracy of the distance determination (≈ 0.05 Å) relative to the bulk spacing (1.92 Å).

Finally, we discuss the static structural disorder, which—as discussed before—is a consequence of projecting the c -(10×2) onto a p -(1×2) unit cell. It is expressed by the anisotropic atomic displacement factor $T(hkl)$ [26]. $T(hkl)$ is given by $T(hkl) = \exp[-2\pi^2(U_{11}h^2a^{*2} + U_{22}k^2b^{*2} + U_{33}l^2c^{*2})]$, where the U_{ii} are the mean squared displacement amplitudes along the a , b , and c directions, respectively.

The positions of the Co and oxygen atoms in the CoO films exhibit substantial modulation which is most pronounced along the [110] direction with values up to $\sqrt{U_{11}} = 0.54 \text{ \AA}$ for the second layer Co atoms and $\sqrt{U_{11}} = 0.30 \text{ \AA}$ to 0.35 \AA for the first-layer Co atoms and all oxygen atoms. These huge values come not unexpectedly when comparison is made with the LEED analysis of the single-bilayer film [1] in which for the c -(10 \times 2) unit cell variations of atomic positions in the range of 0.5 \AA are reported. Along the $[1\bar{1}0]$ direction, disorder is less important in general with $\sqrt{U_{22}}$ values in the 0.1 \AA to 0.2 \AA range. Finally, the vertical ‘‘rumpling’’ is large in the first bilayer next to the Ir surface ($\sqrt{U_{33}} = 0.10 \text{ \AA}$ to 0.14 \AA), but rapidly decreasing to the second bilayer ($\sqrt{U_{33}} = 0.03 \text{ \AA}$ to 0.07 \AA). In this respect the bilayer films are notably different from the single-layer films where, related to the simultaneous presence of h-BN and RS type patches, huge vertical corrugation ($\approx 1 \text{ \AA}$) is present. This goes in parallel with the general result of the structure analysis that the transition from the single-layer to the bilayer structure involves a significant reorganization of the interface layer to the WZ-type structure.

B. Stress measurement and misfit stress

We measure the stress in double-bilayer thin epitaxial CoO(111) film by exploring the stress-induced curvature of a 0.1 mm thin Ir(001) substrate [25]. We prepare first an epitaxial 2 ML thin Co film on Ir(100), and measure the film stress during Co growth at 300 K , as shown in Fig. 8(a). The plot indicates a tensile stress change $\Delta\tau$ of $+2.6 \text{ N/m}$ after deposition of 2 ML Co. The slope of the stress curve reaches a value of $+17 \text{ GPa}$. The LEED pattern of the inset in Fig. 8(a) shows a (1×1) structure, indicative of pseudomorphic growth of 2 ML Co. The epitaxial misfit η between fcc-Co and Ir is calculated from the respective lattice constants ($a_{\text{Ir}} = 3.839 \text{ \AA}$, $a_{\text{fcc-Co}} = 3.55 \text{ \AA}$) as $\eta = (a_{\text{Ir}} - a_{\text{fcc-Co}})/a_{\text{fcc-Co}} = +8.1\%$. This misfit induces a film stress in the Co film of $\tau = \eta Y/(1 - \nu) = +15.4 \text{ GPa}$, where we use the biaxial Young modulus of fcc-Co $Y/(1 - \nu) = 190 \text{ GPa}$ [33]. This value corresponds within 10% to the slope of the stress curve, and we conclude that the stress in the Co film can be ascribed to its epitaxial misfit.

In order to obtain the CoO(111) film, we oxidize the Co film characterized in Fig. 8(a) by exposing it to oxygen at a partial pressure of $2 \times 10^{-6} \text{ mbar}$ at 600 K . This leads to a compressive stress change, which levels off at -0.5 N/m after an exposure of 400 L [$1 \text{ L} = 1 \text{ Langmuir}$ ($1.33 \times 10^{-6} \text{ mbar s}$)], as shown in Fig. 8(b). At this stage the additional diffraction spots shown in the LEED image of Fig. 8(b) indicate the formation of a c -(10 \times 2) structure, which is ascribed to the formation of two-bilayer CoO(111) [2]. For smaller exposures this structure is not observed. To determine the overall stress change due to the formation of two-layer CoO(111) we add the stress change from the Co growth and the oxidation and obtain a tensile stress of $+2.1 \text{ N/m}$.

This result of a tensile stress clearly disqualifies a bulklike RS structure of the CoO film. That structure would lead to charged Co^{2+} and O^{2-} layers, which would induce compressive stress, in contrast to the experimental finding. Rather, the stress change of $+2.1 \text{ N/m}$ is quantitatively ascribed to

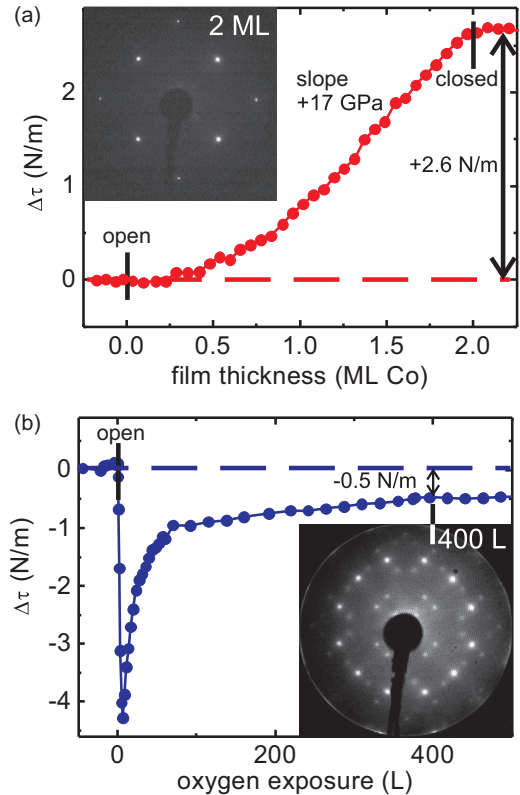


FIG. 8. (Color online) (a) Stress change during growth of 2 ML Co on Ir(100) at 300 K . The inset shows a (1×1) LEED pattern of the resulting structure of 2 ML Co. (b) Stress change during oxidation of the Co film of (a) at 510 K . The LEED pattern of the inset indicates the formation of a c -(10 \times 2) structure of CoO(111) [2]. LEED: Electron energy: 100 eV . The time at which the shutter of the evaporator was opened and closed is indicated.

the epitaxial misfit between the c -(10 \times 2) CoO(111) film and Ir(100), as outlined next.

To calculate the epitaxial misfit stress in the CoO film we need to establish its misfit with respect to the Ir substrate. The structural analysis of the CoO film by LEED in combination with STM [2] and SXRD reveals that the CoO surface unit cell dimensions corresponds to 10 times that of the Ir(001)-(1 \times 1) surface along Ir [110], and twice its length along the perpendicular in-plane direction. We consider that nine nearest-neighbor distances of CoO (27.09 \AA) correspond to 10 nearest-neighbor distances of Ir (27.15 \AA) along the long unit cell direction. This corresponds to an anisotropic in-plane strain of the CoO(111) film, which amounts to $\epsilon_x = +0.22\%$ and $\epsilon_y = +4.2\%$ along the long and short unit cell directions, respectively. An anisotropic film stress results and it is calculated [34,35] as $\tau_x = +0.52 \text{ N/m}$ and $\tau_y = 3.59 \text{ N/m}$ for 2 ML CoO. We observe two structural domains which are rotated by 90° with respect to each other. This results in an average calculated film stress of $\tau_{\text{avg}} = (\tau_x + \tau_y)/2 = +2.05 \text{ N/m}$. This corresponds quantitatively to the measured value, and it supports the view that the film stress is determined by epitaxial misfit, whereas we find no indications for repulsive Coulomb interactions.

To appreciate this result we refer to a recent theoretical work which predicted that ultrathin oxide films of a few layers thickness may be composed of charged layers. The authors argued that the repulsive Coulomb interaction gets prohibitively large only in thicker films [12], where charge compensation mechanisms are expected to stabilize the atomic structure. Our result of a tensile stress suggests that here charge compensation is already active at a thickness of two bilayers.

Our structural analysis presented above suggests that the CoO film can be rather described as a WZ-like and not as a RS structure. One characteristic of the WZ structure here is that adjacent cation and anion layers within one bilayer move towards each other. This may offer a way to reduce, or possibly cancel, the repulsive Coulomb interaction. Such a charge compensation mechanism driven by a structural change has been proposed also for other ionic systems [4,16]. The following discussion of the theoretical results indicates that the CoO film studied here is metallic, not ionic, and this explains the lack of repulsive Coulomb interactions as contributions to film stress.

C. Theory

To study the electronic and magnetic properties of the CoO(111) bilayers on Ir(001) substrate, we carried out extensive first-principles calculations using a Green's function Korrington-Kohn-Rostoker method, which is specially designed for semi-infinite systems such as surfaces and interfaces [36]. We applied the generalized gradient approximation (GGA) for the exchange-correlation functional [37] and the GGA + U approach of Dudarev [38] to describe the localized nature of the Co d states with the effective parameter $U^* = U - J = 1$ eV as was suggested in the previous studies [5,6].

We use the experimentally obtained structural models of 1.6 and 2.0 bilayer CoO(111) films on Ir(001) including four Co atoms in the unit cell as input for our calculations (see Figs. 5–7). We calculated the total energy of various collinear magnetic configurations within the given p -(1 \times 2) unit cell and found that the checkerboard antiparallel alignment of magnetic moments is energetically preferred. It has to be noted that this might not be the ground state, since the calculations were carried out for the small unit cell. Therefore, possible magnetic configurations within the c -(10 \times 2) unit cell were not considered. However, the small unit cell already allows several fundamental statements concerning the electronic and magnetic properties of the system, as was shown by a previous theoretical study [5]. Therefore, we used this configuration as a reference state for the magnetic structure calculations and applied the magnetic force theorem (see discussion below). The density of states (DOS) of this magnetic configuration and the atomic resolved magnetic moments are shown in Fig. 9 and Fig. 10 for the structural models of the 1.6 and 2.0 bilayer film, respectively. The main features of the two DOS are the following.

(i) In all cases, the DOS exhibits a metallic character. This is also valid for a wide range of U^* : $0 < U^* < 6$ eV. We conclude that the thickness of the CoO films is not large enough to open a band gap, which is expected for the wurtzite CoO [39].

(ii) There is a very strong hybridization between oxygen p and Co d states throughout the whole valence band, which we

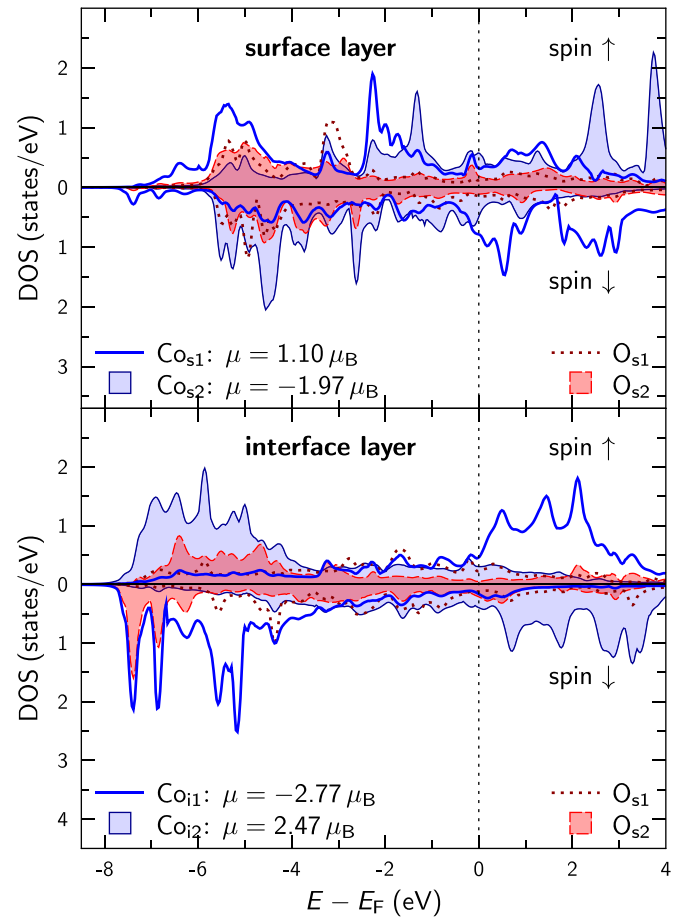


FIG. 9. (Color online) Spin-resolved density of states and the magnetic moments μ of the 1.6 bilayer film. Both layers are plotted, surface (top) and interface (bottom). The Co atoms (blue lines) and O atoms (red lines) of the unit cell are labeled correspondingly to Fig. 5.

ascribe to the shorter distances between Co and O atoms in comparison with bulk CoO (see Fig. 5).

(iii) In general, the magnetic moments (μ) of the Co atoms at the interface to Ir (labeled by Co_{in} , $n = 1$ or 2) are significantly enhanced, which is due to the strong interaction between the electronic states of the Co_{in} and the Ir substrate. The strong interaction leads to a reversed occupation of the d_{z^2} orbitals of the Co_{in} compared to the Co_{sn} . The interfacial Co atoms are located close to the top of the interfacial Ir atoms and, thereby, the d_{z^2} orbitals are more occupied than those in Co bulk. The Co atoms in the surface CoO bilayer experience a very strong interaction with the oxygen atom of the interfacial CoO bilayers. In this case the d_{z^2} orbitals are even more occupied than those at the interface. The strong hybridization between the Co and Ir atoms is responsible for the Co termination at the CoO/Ir(001) interface, which is confirmed by our total energy calculations.

(iv) In the 2.0 bilayer CoO film more d states are occupied than in the 1.6 bilayer case. This is related to the smaller intra-bilayer spacings (0.20 Å vs 0.49 Å and 0.86 Å vs 0.99 Å) leading to a stronger in-plane hybridization of the O p and Co d orbitals and to slightly higher magnetic moments.

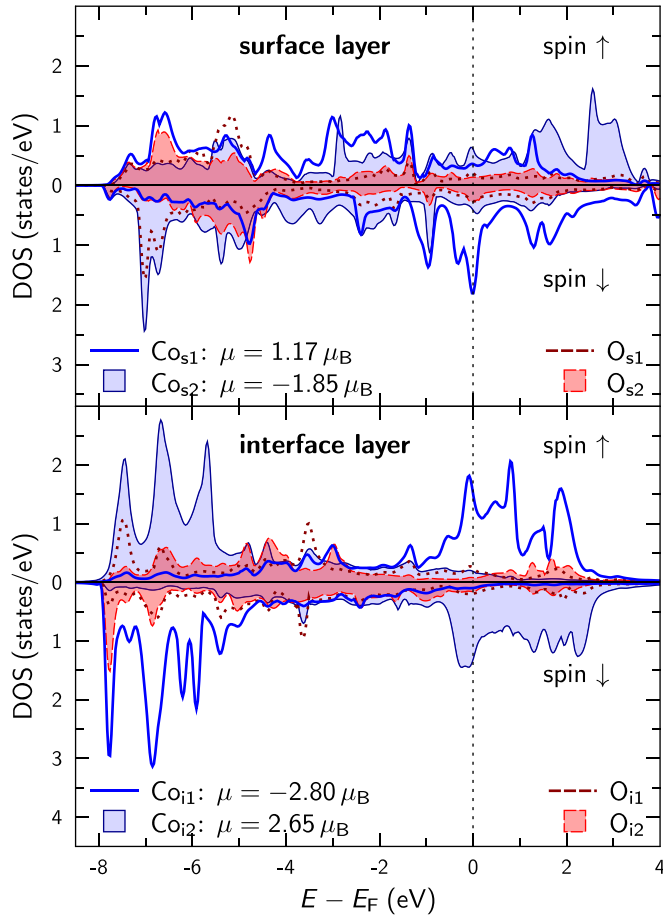


FIG. 10. (Color online) Spin-resolved density of states and the magnetic moments μ of the 2.0 bilayer film. The labels are similar to Fig. 9.

To study the magnetic properties, also the magnetic exchange interactions (J_{ij}) between the Co atoms were calculated. The exchange parameters were obtained using the magnetic force theorem formulated in terms of the multiple scattering theory [40]. This method allows to determine the magnetic order of a system within the smallest unit cell analyzing the exchange interaction between magnetic moments. The details of our magnetic structure simulations can be found in Ref. [41].

The exchange parameters calculated for the checkerboard antiparallel alignment of magnetic moments are presented in Fig. 11 for the 1.6 bilayer (a) and the 2.0 bilayer film (b). These results lead to the following conclusions.

(1) The main exchange interactions in the CoO films are negative (antiferromagnetic), while some J_{ij} vanish or become positive (ferromagnetic) due to large variations in the Co-O bond lengths and the interaction with the underlying quadratic Ir substrate. In comparison with bulk CoO, the interactions are of long range because the typical antiferromagnetic superexchange interaction is suppressed.

(2) The square substrate surface symmetry causes a high anisotropy of the exchange interactions in the quasi-hexagonal CoO layers. The coupling along the [110] direction is strongly antiferromagnetic and symmetric with respect to the $[1\bar{1}0]$

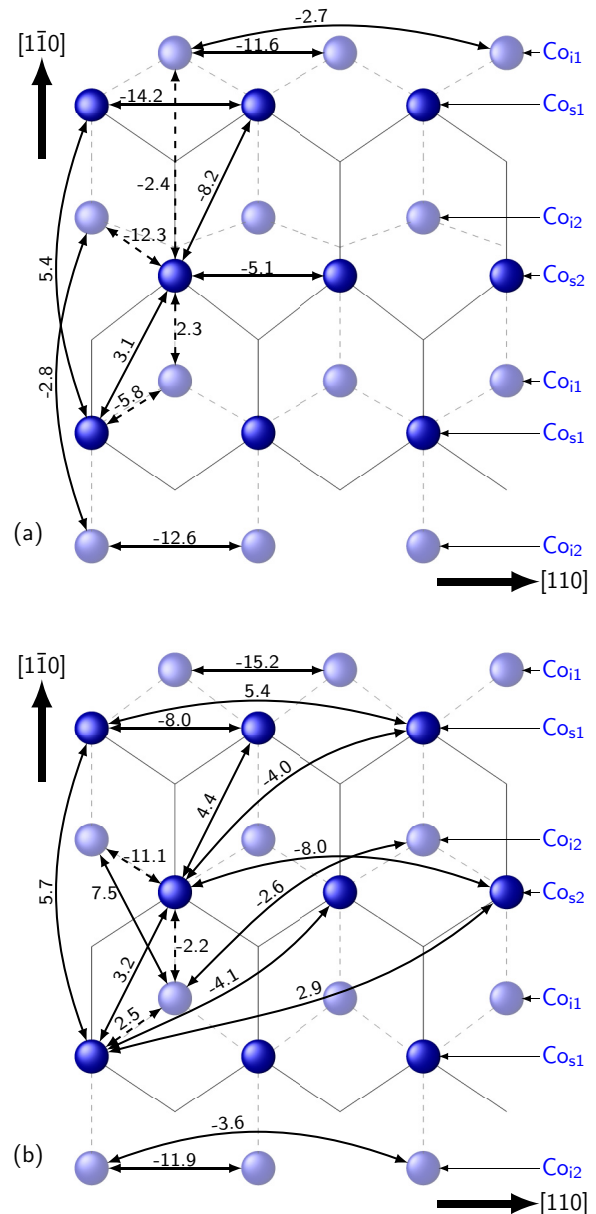


FIG. 11. (Color online) Top view of the structure model of the 1.6 (a) and 2.0 (b) bilayer CoO film on Ir(001) with the most important magnetic exchange interactions J_{ij} . They are shown in solid (dashed) arrows with the value in meV for the in-plane (out-of-plane) interaction. The Co atoms (blue balls) are labeled correspondingly to Fig. 5. Atoms in lighter color are below those represented in darker color. Thin solid (dashed) lines indicate the bonds in the surface (interface) layer.

direction, whereas along the perpendicular direction it is small or even vanishes depending on occupation and layer. Therefore, there exist rows of antiferromagnetically coupled Co atoms along the [110] direction. A similar feature of coupled rows was also observed for the ground state of the CoO monolayer on Ir(001) [5].

In the interface layer (Co_{i1} and Co_{i2}), these rows are coupled in-plane either very weakly or ferromagnetically for the 1.6 bilayer or the 2.0 bilayer film, respectively. This is attributed to the different Co-O bond lengths. For the 2.0 bilayer film, the

bond lengths are 1.88 Å and 1.85 Å, while for the 1.6 bilayer film, the bond along the $[1\bar{1}0]$ direction is strongly elongated to 2.36 Å which reduces the coupling.

(3) For the surface layer, the exchange interactions are much stronger and of longer range compared to those for interface layer. This leads, together with the strong interlayer coupling constants, to a coupling of the interface layer Co atoms and very likely to a noncollinear magnetic structure. We could not identify any commensurate magnetic structure which conforms with the results of Mittendorfer *et al.* [5]; a CoO overlayer on Ir(001) has a noncollinear ordering.

Finally, we use the magnetic exchange interactions in a Heisenberg model and apply a Monte Carlo simulation to determine the magnetic ordering temperature T_c (for details see Ref. [41]). We found a magnetic ordering temperature of 52 K and 90 K for the 1.6 bilayer and the 2.0 bilayer film, respectively. The higher T_c for the 2.0 bilayer film results from the stronger nearest-neighbor exchange interactions. We also estimated the variation of T_c upon allowing for some ($\approx 2\%$ to 3%) variation of the structural parameters, which lies in the range of 4 K to 6 K.

IV. CONCLUSIONS

We have carried out a surface x-ray diffraction study of 1.6 and 2.0 bilayer thick CoO films on Ir(001) prepared by

deposition of Co followed by oxidation at elevated temperature. We find that both films form a wurtzite-like structure similar to the upper four layers of the thicker films studied previously by LEED [4]. Vertical relaxations of the intralayer distance between oxygen and Co atoms are present involving a significant reduction of the dipole moment. This finding also offers an explanation for our stress measurement, where we did not observe any indication for repulsive interaction within the CoO film. Using first-principles calculations, we find that the electronic and magnetic properties of the CoO film on the Ir(100) substrate are strongly influenced by the underlying crystalline structure. Our magnetic structure simulations reveal a noncollinear magnetic order in both systems and highly anisotropic intra- and interlayer exchange interactions due to strong structural modulations. Our calculations reveal a metallic behavior in bilayer CoO films which is also expected to contribute to the polarity compensation in them.

ACKNOWLEDGMENTS

The authors acknowledge support and hospitality by the staff of the ESRF. We thank F. Weiss and N. Kurowsky for technical support. This work is supported by the DFG through SFB 762.

-
- [1] C. Ebensperger, M. Gubo, W. Meyer, L. Hammer, and K. Heinz, *Phys. Rev. B* **81**, 235405 (2010).
- [2] C. Giovanardi, L. Hammer, and K. Heinz, *Phys. Rev. B* **74**, 125429 (2006).
- [3] K. Heinz and L. Hammer, *J. Phys. Condens. Matter* **25**, 173001 (2013).
- [4] W. Meyer, D. Hock, K. Biedermann, M. Gubo, S. Müller, L. Hammer, and K. Heinz, *Phys. Rev. Lett.* **101**, 016103 (2008).
- [5] F. Mittendorfer, M. Weinert, R. Podloucky, and J. Redinger, *Phys. Rev. Lett.* **109**, 015501 (2012).
- [6] C. Toppner, T. Schmitt, M. Reuschl, L. Hammer, M. A. Schneider, F. Mittendorfer, J. Redinger, R. Podloucky, and M. Weinert, *Phys. Rev. B* **86**, 235407 (2012).
- [7] S. I. Csiszar, M. W. Haverkort, Z. Hu, A. Tanaka, H. H. Hsieh, H.-J. Lin, C. T. Chen, T. Hibma, and L. H. Tjeng, *Phys. Rev. Lett.* **95**, 187205 (2005).
- [8] H. N. Ok and J. G. Mullen, *Phys. Rev.* **168**, 550 (1968).
- [9] P. W. Tasker, *J. Phys. C: Solid State Phys.* **12**, 4977 (1979).
- [10] J. Goniakowski, F. Finocchi, and C. Noguera, *Rep. Prog. Phys.* **71**, 016501 (2008).
- [11] C. Noguera, *J. Phys. Condens. Matter* **12**, R367 (2000).
- [12] J. Goniakowski, C. Noguera, and L. Giordano, *Phys. Rev. Lett.* **98**, 205701 (2007).
- [13] J. Goniakowski and C. Noguera, *Phys. Rev. B* **83**, 115413 (2011).
- [14] C. Noguera and J. Goniakowski, *J. Phys. Condens. Matter* **20**, 264003 (2008).
- [15] H. L. Meyerheim, C. Tusche, A. Ernst, S. Ostanin, I. V. Maznichenko, K. Mohseni, N. Jedrecy, J. Zegenhagen, J. Roy, I. Mertig, and J. Kirschner, *Phys. Rev. Lett.* **102**, 156102 (2009).
- [16] C. Tusche, H. L. Meyerheim, and J. Kirschner, *Phys. Rev. Lett.* **99**, 026102 (2007).
- [17] M. De Santis, A. Buchsbaum, P. Varga, and M. Schmid, *Phys. Rev. B* **84**, 125430 (2011).
- [18] S. Ferrer and F. Comin, *Rev. Sci. Instrum.* **66**, 1674 (1995).
- [19] R. Feidenhans'l, *Surf. Sci. Rep.* **10**, 105 (1989).
- [20] *Elements of Modern X-Ray Physics* by J. Als-Nielsen and D. McMorrow (Wiley, West Sussex, UK, 2011), 2nd. ed., p. 169.
- [21] I. K. Robinson and D. J. Tweet, *Rep. Prog. Phys.* **55**, 599 (1992).
- [22] D. Sander, *Curr. Opin. Solid State Mater. Sci.* **7**, 51 (2003).
- [23] D. Sander, Z. Tian, and J. Kirschner, *Sensors* **8**, 4466 (2008).
- [24] A. Dhaka, D. Sander, H. L. Meyerheim, K. Mohseni, E. Soyka, J. Kirschner, W. A. Adeagbo, G. Fischer, A. Ernst, and W. Hergert, *Phys. Rev. B* **84**, 195441 (2011).
- [25] Z. Tian, Ph.D. thesis, Martin Luther University Halle-Wittenberg, 2008.
- [26] W. F. Kuhs, *Acta Crystallogr. Sect. A* **48**, 80 (1992).
- [27] H. L. Meyerheim, Habilitationsschrift zur Erlangung der Venia Legendi, Ludwig-Maximilians-Universität München.
- [28] I. K. Robinson in *Handbook of Synchrotron Radiation*, edited by G. S. Brown and D. E. Moncton (Elsevier, Amsterdam, 1991), Vol. 3.
- [29] U. H. Zucker, E. Perenthaler, W. F. Kuhs, R. Bachmann, and H. Schulz, *J. Appl. Crystallogr.* **16**, 358 (1983).
- [30] $R_u = \frac{\sum |I_{\text{obs}} - I_{\text{calc}}|}{\sum I_{\text{obs}}}$ GOF = $\frac{\sum [(I_{\text{obs}} - I_{\text{calc}})^2 / \sigma^2]}{[1/(N - P)]}$. Here, I_{obs} , I_{calc} , are the experimental and calculated intensities from superlattice structure, respectively, while N and P represent the number of data points and the number of refined parameters. The standard deviation of I_{obs} is given by σ . The summation runs over all data points.

- [31] A. Risbud, L. P. Snedeker, M. M. Elcombe, A. K. Cheetam, and R. Seshadri, *Chem. Mater.* **17**, 834 (2005).
- [32] W. Meyer, Ph.D. thesis, Universität Erlangen-Nürnberg, 2009.
- [33] D. Sander, S. Ouazi, V. Stepanyuk, D. Bazhanov, and J. Kirschner, *Surf. Sci.* **512**, 281 (2002).
- [34] R. F. S. Hearmon, in Landolt-Börnstein, Group 3, Vol. 18, *The Elastic Constants of Crystals and Other Anisotropic Materials* (Springer, Berlin, 1984).
- [35] D. Sander, *Rep. Prog. Phys.* **62**, 809 (1999).
- [36] M. Lüders, A. Ernst, W. Temmerman, Z. Szotek, and P. J. Durham, *J. Phys. Condens. Matter* **13**, 8587 (2001).
- [37] J. P. Perdew, K. Burke, and M. Ernzerhof, *Phys. Rev. Lett.* **77**, 3865 (1996).
- [38] S. L. Dudarev, G. A. Botton, S. Y. Savrasov, C. J. Humphreys, and A. P. Sutton, *Phys. Rev. B* **57**, 1505 (1998).
- [39] M. J. Han and J. Yu, *J. Korean Phys. Soc.* **48**, 1496 (2006).
- [40] A. I. Liechtenstein, M. I. Katsnelson, V. P. Antropov, and V. A. Gubanov, *J. Magn. Magn. Mater.* **67**, 65 (1987).
- [41] G. Fischer, M. Däne, A. Ernst, P. Bruno, M. Lueders, Z. Szotek, W. M. Temmerman, and W. Hergert, *Phys. Rev. B* **80**, 014408 (2009).